Photocurrent Induced by a Bicircular Light Drive in Centrosymmetric Systems

Yuya Ikeda, Sota Kitamura, and Takahiro Morimoto
Department of Applied Physics, The University of Tokyo, Hongo, Tokyo 113-8656, Japan

A bicircular light (BCL) consists of left and right circularly polarized lights with different frequencies, and draws a roselike pattern with a rotational symmetry determined by the ratio of the two frequencies. Here we show that an application of a BCL to centrosymmetric systems allows a photocurrent generation through introduction of an effective polarity to the system. We derive formulas for the BCL-induced photocurrent from a standard perturbation theory, which is then applied to a simple 1D model and 3D Dirac and Weyl semimetals. A nonperturbative effect with strong light intensity is also discussed with the Floquet technique.

Introduction.—Symmetry plays a central role in studying quantum phases of matter and governs their responses to external perturbations [1]. For example, time-reversal symmetry breaking allows quantum Hall effects with quantized Hall conductivity [2]. Inversion symmetry breaking is necessary for the emergence of electric polarization [3] and the bulk photovoltaic effect [4]. Symmetry of the electronic system in solids is usually determined by the crystal structure, spontaneous symmetry breaking in the ground state such as magnetic order, and an application of the external field.

Dynamical control of quantum systems by periodic driving has attracted keen attention and is currently called "Floquet engineering" [5–7]. Periodic driving has an advantage that it can control the symmetry and topology of quantum materials without changing their chemical composition and sometimes offers novel quantum phases which have no counterpart in the equilibrium [8–12]. In particular, an application of the circularly polarized light (CPL) can introduce an effective time-reversal symmetry (TRS) breaking to the system, which is exemplified by the emergence of an anomalous Hall insulating phase in graphene under CPL [13,14].

Employing a two-frequency drive instead of a monochromatic drive has recently been attracting an interest as a method to enlarge the capabilities of Floquet engineering [15–21]. In particular, the spatial inversion symmetry and rotational symmetry of the system can be controlled by applying so called bicircular light (BCL). The BCL consists of two CPL waves with different frequencies and opposite chirality [22], and is expressed in the form of a vector potential as

$$A_x(t) + iA_y(t) = A_0[e^{in_1\Omega t} + e^{-in_2\Omega t + i\theta}], \quad (1)$$

where A_0 is the amplitude and n_1, n_2 are the integers representing the frequencies of the two CPL waves. The BCL wave draws the roselike pattern with $(n_1 + n_2)/\gcd(n_1, n_2)$-fold rotational symmetry as shown in Fig. 1(a), which implies that applying BCL can reduce the system's rotational symmetry from that of the crystal structure. The parameter θ is the phase difference between two CPL waves and serves as a knob to rotate the rose pattern drawn by the BCL wave [see Fig. 1(b)]. Recently, several studies on the control of symmetry and topology using a BCL drive have been reported, including charge dynamics in graphene [23] and Weyl point generation in Dirac semimetals [24].
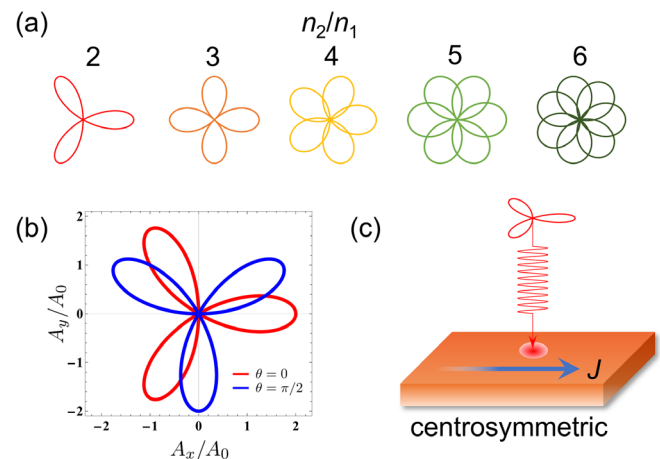
FIG. 1. Schematics of bicircular light (BCL) that consists of circularly polarized light (CPL) with different frequencies. (a) The electric field of the BCL draws the roselike pattern with a rotational symmetry determined by the ratio of the two frequencies. The rose patterns with $n_1 = 1$, $n_2 = n$ in Eq. (1) are plotted. (b) The relative phase between two CPL waves leads to rotation of the rose pattern of the BCL. (c) Application of BCL to centrosymmetric systems can induce a photocurrent with the introduction of an effective polarity.

Moreover, it was also shown that the BCL driving can introduce polarity in centrosymmetric systems and induce electric polarization due to inversion symmetry breaking originating from incompatible rotation symmetry of the BCL [25].

BCL's ability to control the inversion and rotation symmetry of the materials is also expected to apply to optoelectronic properties of materials. In particular, the bulk photovoltaic effect (BPVE) [4] is an important non-linear optical phenomenon in a system lacking inversion symmetry, where the light irradiation induces a dc photo-current [26–28]. There are several mechanisms for the BPVE, including the shift current, injection current, and ballistic current [29–31]. Among them, the injection current is a photocurrent proportional to the relaxation time of photocarriers and plays a dominant role in the circular photogalvanic effect in which circularly polarized light induces a chirality dependent photocurrent [31]. Indeed, the application of a two-frequency drive has been studied as a method to induce the injection current [32] and injection spin current [33] based on a perturbation theory, showing a coherent control of the current direction with the relative phase of the two frequency lights. Such coherent control of a photocurrent was demonstrated in Bi_2Se_3 in a collinear polarization scheme [34]. More recently, a photocurrent induced by corotating CPL in the strong intensity regime has been studied with an *ab initio* calculation [35].

In this Letter, we study a photocurrent induced by the BCL, on the basis of Floquet engineering of inversion and rotational symmetries of the system. We demonstrate that irradiating the C_3-symmetric BCL creates a photocurrent in inversion symmetric systems such as C_2 or C_4 symmetric systems [Fig. 1(c)], where the photocurrent cannot be induced by conventional monochromatic light irradiation. Specifically, using the perturbation theory and the Floquet theory, we derive a formula for the BCL-induced photo-current which is proportional to the relaxation time τ (i.e., injection current) in systems with spatial symmetries. We apply the obtained formula to a 1D system with inversion symmetry and a 3D Dirac or Weyl semimetal, where the latter exhibits a large photocurrent due to its gapless nature. The direction of the photocurrent can be controlled by the pattern of the BCL light through the phase θ. Also, non-perturbative effects on the photocurrent with the light intensity are discussed with the Floquet-Keldysh formalism.

BCL-induced photocurrent.—Let us study a photocurrent induced by a BCL drive in centrosymmetric systems based on a standard perturbation theory. Specifically, we adopt a diagrammatic approach [36] to calculate the nonlinear optical conductivity for the BCL-induced photocurrent. Under the vector potential $A(t)$ of the BCL, the dynamics of the electron obeys the time-dependent Schrödinger equation with the time-dependent Hamiltonian $H(t)$ with minimal coupling,

$$H(t) = H_0(\boldsymbol{k} + e\boldsymbol{A}(t)/\hbar), \qquad (2)$$

where $H_0(\boldsymbol{k})$ is the Bloch Hamiltonian in the equilibrium. In the following, we focus on the C_3-symmetric BCL repre-sented by $\boldsymbol{A}(t) \equiv [A_x(t), A_y(t)]$ with $(n_1, n_2) = (1, 2)$ in Eq. (1). The electric field is given by $\boldsymbol{E}(t) = -\partial\boldsymbol{A}(t)/\partial t \equiv \text{Re}[\boldsymbol{E}^{(\Omega)}e^{i\Omega t} + \boldsymbol{E}^{(-2\Omega)}e^{-2i\Omega t}]$, with the com-plex electric fields $\boldsymbol{E}^{(\Omega)}$ and $\boldsymbol{E}^{(-2\Omega)}$. BCL driving breaks both time-reversal symmetry and spatial symmetries inclu-ding inversion, which leads to a photocurrent generation even in systems with spatial inversion or rotational sym-metry. Specifically, the BCL-induced photocurrent is a third-order response with respect to the electric field at the lowest order as with the combination of the photon ener-gies, $\Omega + \Omega - 2\Omega = 0$. The dominant contribution to the photocurrent is the so-called injection current contribution which is proportional to the relaxation time $\tau \sim \hbar/\gamma_0$. In the diagrammatic approach, such contribution is included in the box diagram as detailed in the Supplemental Material [37]. By keeping only the terms $\propto 1/\gamma_0$ in the diagrammatic computation, we obtain the expression for the BCL-induced photocurrent as

$$J_{\text{BCL}}^{\mu\alpha\beta\gamma}(\Omega) = \text{Re}[\sigma_{\text{BCL}}^{\mu\alpha\beta\gamma}E_\alpha^{(\Omega)}E_\beta^{(\Omega)}E_\gamma^{(-2\Omega)}] \qquad (3)$$

with

$$\sigma_{\text{BCL}}^{\mu\alpha\beta\gamma} \simeq \frac{i\pi e^4}{3\hbar^4\Omega^3\gamma_0} \sum_{\substack{\{\alpha,\beta,\gamma\}\\a,b,c}} \int [d\boldsymbol{k}]f_{ab}(v_{aa}^\mu - v_{bb}^\mu)$$

$$\times \left[\left(\frac{v_{ac}^\alpha v_{cb}^\beta v_{ba}^\gamma}{\epsilon_{ac} + 2\hbar\Omega} + \frac{v_{ac}^\alpha v_{cb}^\beta v_{ba}^\gamma}{\epsilon_{ac} - \hbar\Omega} \right) \delta(\epsilon_{ab} + \hbar\Omega) \right.$$

$$\left. + \frac{v_{ca}^\alpha v_{bc}^\beta v_{ab}^\gamma}{\epsilon_{ac} + \hbar\Omega} \delta(\epsilon_{ab} + 2\hbar\Omega) \right], \qquad (4)$$

where we defined $[d\boldsymbol{k}] \equiv d\boldsymbol{k}/(2\pi)^d$ with the spatial dimen-sion d, $\epsilon_{ab} = \epsilon_a - \epsilon_b$ and $f_{ab} = f(\epsilon_a) - f(\epsilon_b)$ represent the difference of band energies and the Fermi distribution functions, respectively, and $v_{ab}^\alpha = \langle a|(\partial H_0/\partial k_\alpha)|b\rangle$ repre-sents the matrix element of the velocity operator. Here we defined $\sigma_{\text{BCL}}^{\mu\alpha\beta\gamma} \equiv \sum_{\{\alpha,\beta,\gamma\}} \sigma^{\mu\alpha\beta\gamma}(0; \Omega, \Omega, -2\Omega)$ by adding up the nonlinear conductivities $\sigma^{\mu\alpha\beta\gamma}$ in all possible permuta-tions of $\{\alpha, \beta, \gamma\}$, e.g., $\sigma_{\text{BCL}}^{xxyy} = \sigma^{xxyy} + \sigma^{xyxy} + \sigma^{xyyx}$. This simplifies the expression due to some cancellations between different tensor elements $\sigma^{\mu\alpha\beta\gamma}$. We note that the above expression is only valid when the photocurrent is generated by the C_3-symmetric BCL driving and $E_\alpha^{(\Omega)}E_\beta^{(\Omega)}E_\gamma^{(-2\Omega)}$ remains the same value regardless of the permutations of

the spatial indices $\{\alpha, \beta, \gamma\}$ because $\boldsymbol{E}^{(\Omega)}$ and $\boldsymbol{E}^{(-2\Omega)}$ are proportional to each other.

In the two-band limit ($n = 1, 2$), the expressions for $J^x(\Omega)$ and $J^y(\Omega)$ reduce to

$$
\begin{aligned}
J^\alpha_{\mathrm{BCL}}(\Omega) = & \frac{2\pi e^4 A_0^3}{3\hbar^5 \Omega \gamma_0} C \int [d\boldsymbol{k}] f_{12} \Delta v^\alpha \\
& \times [(|v_{12}^x|^2 - |v_{12}^y|^2)\Delta v^\alpha + 2s\mathrm{Re}[v_{12}^x v_{21}^y]\Delta v^\beta] \\
& \times \left(-\frac{1}{2}\delta(\epsilon_{12} + \hbar\Omega) + \delta(\epsilon_{12} + 2\hbar\Omega)\right),
\end{aligned} \quad (5)
$$

with $(\alpha, \beta, C, s) = (x, y, \cos\theta, -1)$ for J^x and $(\alpha, \beta, C, s) = (y, x, \sin\theta, 1)$ for J^y. Here, $\Delta v^\alpha = (v_{11}^\alpha - v_{22}^\alpha)$ is the group velocity difference for the two bands. In particular, the above expression clearly indicates that one can control the direction of the photocurrent by tuning the phase difference θ since $J^x_{\mathrm{BCL}} \propto \cos\theta$ and $J^y_{\mathrm{BCL}} \propto \sin\theta$.

Applications to 1D SSH model and 3D Dirac and Weyl semimetals.—To demonstrate the BCL-induced photocurrent, we first apply the above formula to the 1D Su-Schrieffer-Heeger (SSH) model, which we adopt as a simple 1D model for systems with inversion symmetry and is described by the Hamiltonian (we set lattice constant to be $a = 2$),

$$
H(k) = 2t_0 \cos k\sigma_x - 2\delta t_0 \sin k\sigma_y, \quad (6)
$$

where $t_0 \pm \delta t_0$ is the amplitude of the nearest neighbor hopping with bond alternation and σ_i ($i = x, y, z$) are Pauli matrices [Fig. 2(a)]. The energy dispersion is given by $E(k) = \pm\sqrt{4t_0^2\cos^2 k + 4\delta t_0^2\sin^2 k}$ as plotted in Fig. 2(b).
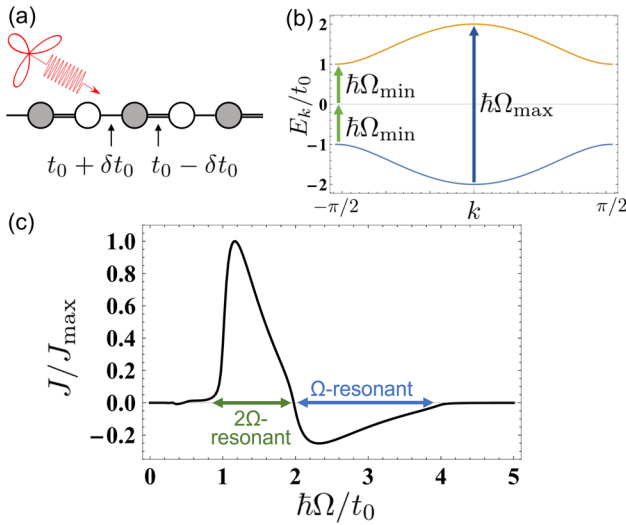
FIG. 2. A BCL-induced photocurrent in the 1D SSH model. (a) A schematic picture of the SSH model driven by threefold BCL. (b) The band dispersion of the SSH model. The minimum (maximum) input frequency $\Omega_{\min}$ ($\Omega_{\max}$) is depicted with the green (blue) arrow. (c) Photocurrent dependence on the input frequency (we set $\delta t_0 = 0.5t_0$).

We note that $H(k)$ has an inversion symmetry, i.e., $\sigma_x H(k)\sigma_x = H(-k)$ which prohibits the conventional second order contribution to the photocurrent and makes the BCL-induced photocurrent a dominant contribution.

Using the formula for two-band systems in Eq. (5), we obtain the photocurrent for the SSH model under the BCL as

$$
\begin{aligned}
J_{\mathrm{BCL}}(\Omega) = & \frac{2\pi e^4 A_0^3}{3\hbar^5 \Omega \gamma_0} \cos\theta \int [dk]|v_{12}|^2 (v_{11} - v_{22})^2 \\
& \times \left(-\frac{1}{2}\delta(\epsilon_{12} + \hbar\Omega) + \delta(\epsilon_{12} + 2\hbar\Omega)\right).
\end{aligned} \quad (7)
$$

This shows that the photocurrent induced by BCL driving involves two interband resonance terms: the Ω-resonant term $\propto \delta(\epsilon_{12} + \hbar\Omega)$ and the 2Ω-resonant term $\propto \delta(\epsilon_{12} + 2\hbar\Omega)$ with a sign change. Figure 2(c) shows the photocurrent induced by BCL driving in the 1D SSH model when the Fermi energy lies within the energy gap. For $|\delta t_0| < |t_0|$, the photoexcitation by BCL driving occurs in the region $2|\delta t_0| \le \hbar\Omega \le 2|t_0|$ due to the 2Ω-resonant term, and $4|\delta t_0| \le \hbar\Omega \le 4|t_0|$ due to the Ω-resonant term. The directions of the photocurrent are opposite for the two regions reflecting the relative sign in the two delta functions in Eq. (7). The minimum and maximum frequencies for photocurrent generation are given by $\hbar\Omega_{\min} = 2|\delta t_0|$ and $\hbar\Omega_{\min} = 4|t_0|$. Also, we find that the intensity of the first peak is 4 times larger than the second one due to the $1/\Omega$ term in Eq. (7).

Next we study the BCL-induced photocurrent in 3D Dirac and Weyl semimetals which host gapless linear dispersions. For simplicity, we consider a model of a single Weyl fermion with anisotropic velocity along the z direction,

$$
H = \hbar v_F (k_x\sigma_x + k_y\sigma_y + \eta k_z\sigma_z). \quad (8)
$$

Here v_F is a Fermi velocity and η denotes the anisotropy along the z direction. This model has twofold rotational symmetry along the y direction C_2^y. Thus, irradiation of C_3-symmetric BCL perpendicular to the (010) surface induces the photocurrent in the x-z plane. From the two-band formula (5), we obtain

$$
\begin{aligned}
\begin{pmatrix} J^x_{\mathrm{BCL}}(\Omega) \\ J^z_{\mathrm{BCL}}(\Omega) \end{pmatrix} = & \frac{4e^4|v_F|E_0^3}{45\pi\gamma_0\hbar^2\Omega^2} \frac{1 - \eta^2}{|\eta|} \\
& \times \left[-\Theta(\hbar\Omega - |\epsilon_F|) + \frac{1}{8}\Theta(\hbar\Omega - 2|\epsilon_F|)\right] \\
& \times \begin{pmatrix} \cos\theta \\ \eta^2\sin\theta \end{pmatrix},
\end{aligned} \quad (9)
$$

where $\Theta(x)$ is the step function. Note that when the anisotropy is absent with $\eta^2 = 1$, the system has continuous rotational symmetry. In this case, the overall driven system still possesses the C_3^y symmetry of the BCL and the photocurrent vanishes. For a finite chemical potential, the
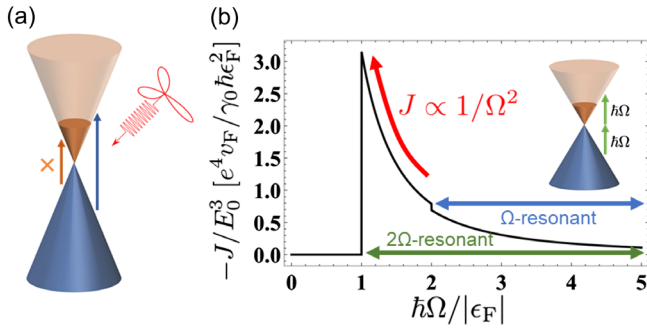
FIG. 3. The BCL-induced photocurrent in Dirac and Weyl semimetals. (a) A schematic picture of a single Dirac cone driven by threefold BCL. Pauli blocking prohibits the photoexcitation with the Ω (2Ω) resonant process for frequencies $\hbar\Omega < 2|\epsilon_F|$ ($2\hbar\Omega < 2|\epsilon_F|$) with the chemical potential ϵ_F. The orange line indicates Pauli blocking for the Ω-resonant process. (b) Photocurrent dependence on the frequency. We set $\eta = 0.8$. The green (blue) arrow represents the frequency range where the Ω (2Ω) resonant process is allowed.

photoabsorption occurs only in the range $\hbar\Omega > |\epsilon_F|$ due to the Pauli blocking. The photocurrent behaves as $J \propto 1/\Omega^2$ with the input light frequency Ω. Since Weyl and Dirac semimetals are gapless, this suggests an enhancement of the photocurrent by applying the BCL wave in the low frequency region, as shown in Fig. 3. Also the direction of the photocurrent can be controlled with the phase θ of BCL, where (J^x, J^z) draws an ellipse by changing the relative phase θ with the ratio of the minor and major axes being η^2. Since this photocurrent is independent of the sign of the Weyl charge [i.e., $\mathrm{sgn}(\eta)$], the photocurrent simply doubles in the Dirac semimetals.

Nonperturbative effects with the Floquet approach.— Next let us study nonperturbative effects for the BCL-induced photocurrent by using an approach based on the Floquet theory. The Floquet theory describes periodically driven systems by an effective band theory with a Floquet Hamiltonian. The Floquet approach for nonlinear optical responses treats the optical resonance as a nonequilibrium steady state realized at an anticrossing of the Floquet bands, and is able to incorporate nonperturbative effects with respect to the electric field that cannot be captured by the diagrammatic approach [38].

We study the nonperturbative effect focusing on the SSH model driven by the C_3-symmetric BCL. The nonequilibrium steady state given by the time-dependent Hamiltonian $H(t) = H_0(k + eA(t)/\hbar)$ with the vector potential of the C_3-symmetric BCL can be described by the following block of the Floquet Hamiltonian:

$$\mathcal{H}_F = \begin{pmatrix} H_0 + 2\hbar\Omega & A'v & A'e^{-i\theta}v \\ A'v & H_0 + \hbar\Omega & A'v \\ A'e^{i\theta}v & A'v & H_0 \end{pmatrix}, \quad (10)$$

with $A' = eA_0/2\hbar$. Here, we consider Floquet bands made of photon-dressed states with 0, 1, and 2 photons, since the C_3-symmetric BCL includes Ω and 2Ω frequency components. The photocurrent in the driven system can be obtained by computing $ie\mathrm{Tr}(v_F G^<)/\hbar$ as detailed in the Supplemental Material. The lesser Green's function $G^<$ encodes the information of the occupation of the Floquet bands, where the nonequilibrium distribution function of electrons is stabilized by attaching an effective particle bath to the system. The current operator under the driving v_F is defined as $v_F = \partial\mathcal{H}_F/\partial k$ when $\mathcal{H}_F$ is represented with k-independent basis.

The photocurrent in the driven systems includes several contributions depending on which Floquet bands are involved in photoexcitation. One typical contribution for the photocurrent from the 2Ω-resonant process is obtained by focusing on three Floquet bands that consist of the valence band with one photon, the valence band with two photons, and the conduction band, which reads

$$J = \frac{2\pi e A'^3}{\hbar^2\Omega} \cos\theta \int [dk] \frac{|v_{12}|^2 v_{11}(v_{11} - v_{22})}{\gamma'} \delta(\epsilon_{12} + 2\hbar\Omega), \tag{11}$$

$$\gamma' = \sqrt{\left| A'e^{-i\theta}v_{12} + \frac{A'^2}{\hbar\Omega}v_{11}v_{12} \right|^2 + \gamma_0^2}, \tag{12}$$

where γ' is the effective relaxation rate in the presence of the BCL with γ_0 being the relaxation rate from the fermionic heat bath (for details of the derivation, see the Supplemental Material). The factor A'^3/γ' gives a nonperturbative effect with respect to E. This leads to a saturation of the photocurrent for large light intensity, with a crossover from $J \propto A_0^3/\gamma_0$ to $J \propto A_0^n$. The exponent n in the high intensity region is expected to depend on which term in $|\cdots|^2$ becomes dominant in Eq. (12). While we have discussed the contribution from a specific three-band model in Eq. (11), contributions from other combinations of Floquet bands also show similar crossover behaviors. In addition, by adding up all the contributions and focusing on the leading order in E, we can reproduce the formula for the BCL-induced photocurrent that was derived from the diagrammatic approach (for details of the full Floquet formulation, see the Supplemental Material).

Application of the above Floquet formulation to the 1D SSH model shows a nonperturbative correction to the photocurrent (Fig. 4). Figure 4(a) shows the amplitude dependence of the photocurrent with several relaxation rate values γ_0. At small γ_0, the crossover of the photocurrent from $J \propto A_0^3/\gamma_0$ to $J \propto A_0^{1.7}$ occurs as shown in Fig. 4(b). The exponent 1.7 in the high intensity region falls in between 1 and 2 as expected from Eq. (12). We note that the present Floquet approach can be also applied to 2D and 3D
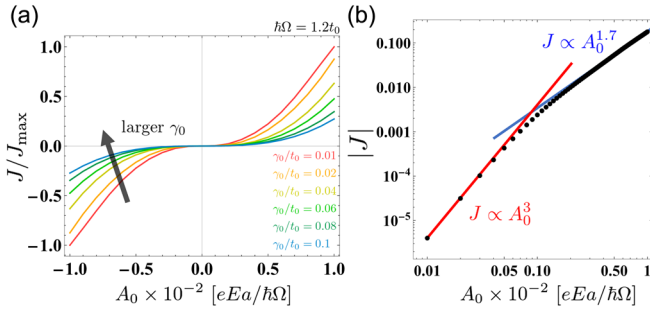
FIG. 4. Nonperturbative effect on the BCL-induced photocurrent. (a) The amplitude dependence of the photocurrent with several relaxation rate values γ_0. (b) The amplitude dependence of the photocurrent at $\gamma_0/t_0 = 0.02$ with fitting curves of $J \propto A_0^3$ (red line) and $J \propto A_0^{1.7}$ (blue line). We set $\hbar\Omega/t_0 = 1.2$.

systems, where the BCL-induced photocurrent is obtained in a similar way and shows a similar saturation effect.

Discussions.—The BCL-induced photocurrent is a third order response with respect to the electric field, $J \propto A^3$, as seen in Eq. (5). While the presence of inversion symmetry forbids the second order responses such as the BPVE with monochromatic light, the third order responses are not forbidden in centrosymmetric systems generally. In this regard, the appearance of the BCL-induced photocurrent does not contradict the presence of inversion symmetry in the unperturbed system. Our finding is that application of the BCL introduces a polarity to the centrosymmetric system and the phase of the two frequency lights can control the direction of the polarity, and hence, the photocurrent. Such controllability of BCL paves a novel venue for searching optoelectronic functionality.

Since Dirac and Weyl semimetals show a diverging photocurrent at low frequencies, those topological semimetals are a promising platform to observe the BCL-induced photocurrent. In particular, a tetragonal 3D Dirac semimetal Cd_3As_2 [39,40] and a hexagonal 3D Dirac semimetal Na_3Bi [41] will be good candidate materials. Both materials host 3D Dirac fermions with anisotropic Fermi velocities along the z direction and the anisotropies are reported to be $\eta \sim 0.25$. In these cases, the magnitude of the BCL-induced photocurrent density is estimated as $J \sim 10^6$ A/m^2 with realistic parameters $\hbar\Omega = 0.1$ eV, $E_0 = 1$ kV/cm, $v_F = 10^6$ m/s, and $\tau = \hbar/\gamma_0 = 1$ ps. Considering a sample with the width $L = 100$ μm and penetration depth $\delta = 1$ μm, the magnitude of the photocurrent is estimated as $I = JL\delta \sim 100$ μA, which gives a large photocurrent in the midinfrared region. Such enhancement of J originates from the gapless nature of Dirac semimetals. Finally, the field strength exhibiting the crossover due to the nonperturbative effect can be estimated as follows. From Fig. 4(b), we can estimate the value at which the photocurrent begins to deviate from $J \propto A_0^3$ as $A_0 \sim 0.01[eE_0a/\hbar\Omega]$ corresponding to $E_0 = 0.4$ MV/cm with a

typical lattice constant $a = 3$ Å and a photon energy $\hbar\Omega = 1.2$ eV.

[1] C.-K. Chiu, J. C. Y. Teo, A. P. Schnyder, and S. Ryu, Classification of topological quantum matter with symmetries, Rev. Mod. Phys. **88,** 035005 (2016).

[2] N. Nagaosa, J. Sinova, S. Onoda, A. H. MacDonald, and N. P. Ong, Anomalous Hall effect, Rev. Mod. Phys. **82,** 1539 (2010).

[3] R. Resta, Macroscopic polarization in crystalline dielectrics: The geometric phase approach, Rev. Mod. Phys. **66,** 899 (1994).

[4] P. J. Sturman and V. M. Fridkin, *Photovoltaic and Photo-Refractive Effects in Noncentrosymmetric Materials* (CRC Press, Philadelphia, 1992), Vol. 8.

[5] T. Oka and S. Kitamura, Floquet engineering of quantum materials, Annu. Rev. Condens. Matter Phys. **10,** 387 (2019).

[6] M. S. Rudner and N. H. Lindner, Band structure engineering and non-equilibrium dynamics in floquet topological insulators, Nat. Rev. Phys. **2,** 229 (2020).

[7] A. Eckardt, Colloquium: Atomic quantum gases in periodically driven optical lattices, Rev. Mod. Phys. **89,** 011004 (2017).

[8] N. H. Lindner, G. Refael, and V. Galitski, Floquet topological insulator in semiconductor quantum wells, Nat. Phys. **7,** 490 (2011).

[9] M. S. Rudner, N. H. Lindner, E. Berg, and M. Levin, Anomalous Edge States and the Bulk-Edge Correspondence for Periodically Driven Two-Dimensional Systems, Phys. Rev. X **3,** 031005 (2013).

[10] X.-X. Zhang, T. T. Ong, and N. Nagaosa, Theory of photoinduced floquet Weyl semimetal phases, Phys. Rev. B **94,** 235137 (2016).

[11] H. Hu, B. Huang, E. Zhao, and W. V. Liu, Dynamical Singularities of Floquet Higher-Order Topological Insulators, Phys. Rev. Lett. **124,** 057001 (2020).

[12] S. Kitamura and H. Aoki, Floquet topological superconductivity induced by chiral many-body interaction, Commun. Phys. **5,** 174 (2022).

[13] T. Oka and H. Aoki, Photovoltaic Hall effect in graphene, Phys. Rev. B **79,** 081406(R) (2009).

[14] Y. H. Wang, H. Steinberg, P. Jarillo-Herrero, and N. Gedik, Observation of Floquet-Bloch states on the surface of a topological insulator, Science **342,** 453 (2013).

[15] O. Neufeld, D. Podolsky, and O. Cohen, Floquet group theory and its application to selection rules in harmonic generation, Nat. Commun. **10,** 405 (2019).

[16] J. H. Kang and Y.-i. Shin, Topological floquet engineering of a one-dimensional optical lattice via resonant shaking

with two harmonic frequencies, Phys. Rev. A **102**, 063315 (2020).

[17] M. S. Mrudul, Álvaro Jiménez-Galán, M. Ivanov, and G. Dixit, Light-induced valleytronics in pristine graphene, Optica **8**, 422 (2021).

[18] K. Sandholzer, A.-S. Walter, J. Minguzzi, Z. Zhu, K. Viebahn, and T. Esslinger, Floquet engineering of individual band gaps in an optical lattice using a two-tone drive, Phys. Rev. Res. **4**, 013056 (2022).

[19] J. Minguzzi, Z. Zhu, K. Sandholzer, A.-S. Walter, K. Viebahn, and T. Esslinger, Topological Pumping in a Floquet-Bloch Band, Phys. Rev. Lett. **129**, 053201 (2022).

[20] N. Rana, M. S. Mrudul, and G. Dixit, Generation of Circularly Polarized High Harmonics with Identical Helicity in Two-Dimensional Materials, Phys. Rev. Appl. **18**, 064049 (2022).

[21] Y. Wang, A.-S. Walter, G. Jotzu, and K. Viebahn, Topological floquet engineering using two frequencies in two dimensions, Phys. Rev. A **107**, 043309 (2023).

[22] O. Kfir, P. Grychtol, E. Turgut, R. Knut, D. Zusin, D. Popmintchev, T. Popmintchev, H. Nembach, J. M. Shaw, A. Fleischer, H. Kapteyn, M. Murnane, and O. Cohen, Generation of bright phase-matched circularly-polarized extreme ultraviolet high harmonics, Nat. Photonics **9**, 99 (2015).

[23] T. Nag, R.-J. Slager, T. Higuchi, and T. Oka, Dynamical synchronization transition in interacting electron systems, Phys. Rev. B **100**, 134301 (2019).

[24] T. V. Trevisan, P. V. Arribi, O. Heinonen, R.-J. Slager, and P. P. Orth, Bicircular Light Floquet Engineering of Magnetic Symmetry and Topology and its Application to the Dirac Semimetal cd_3as_2, Phys. Rev. Lett. **128**, 066602 (2022).

[25] Y. Ikeda, S. Kitamura, and T. Morimoto, Floquet engineering of electric polarization with two-frequency drive, Prog. Theor. Exp. Phys. **2022**, 04A101 (2022).

[26] I. Grinberg, D. V. West, M. Torres, G. Gou, D. M. Stein, L. Wu, G. Chen, E. M. Gallo, A. R. Akbashev, P. K. Davies, J. E. Spanier, and A. M. Rappe, Perovskite oxides for visible-light-absorbing ferroelectric and photovoltaic materials, Nature (London) **503**, 509 (2013).

[27] W. Nie, H. Tsai, R. Asadpour, J.-C. Blancon, A. J. Neukirch, G. Gupta, J. J. Crochet, M. Chhowalla, S. Tretiak, M. A. Alam, H.-L. Wang, and A. D. Mohite, Solar cells. high-efficiency solution-processed perovskite solar cells with millimeter-scale grains, Science **347**, 522 (2015).

[28] L. Z. Tan, F. Zheng, S. M. Young, F. Wang, S. Liu, and A. M. Rappe, Shift current bulk photovoltaic effect in polar materials—hybrid and oxide perovskites and beyond, npj Comput. Mater. **2**, 1 (2016).

[29] Z. Dai and A. M. Rappe, Recent progress in the theory of bulk photovoltaic effect, Chem. Phys. Rev. **4**, 011303 (2023).

[30] N. Nagaosa and T. Morimoto, Concept of quantum geometry in optoelectronic processes in solids: Application to solar cells, Adv. Mater. **29**, 1603345 (2017).

[31] J. Orenstein, J. Moore, T. Morimoto, D. Torchinsky, J. Harter, and D. Hsieh, Topology and symmetry of quantum materials via nonlinear optical responses, Annu. Rev. Condens. Matter Phys. **12**, 247 (2021).

[32] R. Atanasov, A. Haché, J. L. P. Hughes, H. M. van Driel, and J. E. Sipe, Coherent Control of Photocurrent Generation in Bulk Semiconductors, Phys. Rev. Lett. **76**, 1703 (1996).

[33] R. D. R. Bhat and J. E. Sipe, Optically Injected Spin Currents in Semiconductors, Phys. Rev. Lett. **85**, 5432 (2000).

[34] D. A. Bas, K. Vargas-Velez, S. Babakiray, T. A. Johnson, P. Borisov, T. D. Stanescu, D. Lederman, and A. D. Bristow, Coherent control of injection currents in high-quality films of Bi_2Se_3, Appl. Phys. Lett. **106**, 041109 (2015).

[35] O. Neufeld, N. Tancogne-Dejean, U. De Giovannini, H. Hübener, and A. Rubio, Light-Driven Extremely Nonlinear Bulk Photogalvanic Currents, Phys. Rev. Lett. **127**, 126601 (2021).

[36] D. E. Parker, T. Morimoto, J. Orenstein, and J. E. Moore, Diagrammatic approach to nonlinear optical response with application to Weyl semimetals, Phys. Rev. B **99**, 045121 (2019).

[37] See Supplemental Material at http://link.aps.org/supplemental/10.1103/PhysRevLett.131.096301 for details of the diagrammatic approach and the Floquet-Keldysh approach.

[38] T. Morimoto and N. Nagaosa, Topological nature of nonlinear optical effects in solids, Sci. Adv. **2**, e1501524 (2016).

[39] M. Neupane, S.-Y. Xu, R. Sankar, N. Alidoust, G. Bian, C. Liu, I. Belopolski, T.-R. Chang, H.-T. Jeng, H. Lin, A. Bansil, F. Chou, and M. Z. Hasan, Observation of a three-dimensional topological Dirac semimetal phase in high-mobility Cd_3As_2, Nat. Commun. **5**, 3786 (2014).

[40] Z. K. Liu, J. Jiang, B. Zhou, Z. J. Wang, Y. Zhang, H. M. Weng, D. Prabhakaran, S.-K. Mo, H. Peng, P. Dudin, T. Kim, M. Hoesch, Z. Fang, X. Dai, Z. X. Shen, D. L. Feng, Z. Hussain, and Y. L. Chen, A stable three-dimensional topological Dirac semimetal Cd_3As_2, Nat. Mater. **13**, 677 (2014).

[41] Z. K. Liu, B. Zhou, Y. Zhang, Z. J. Wang, H. M. Weng, D. Prabhakaran, S.-K. Mo, Z. X. Shen, Z. Fang, X. Dai, Z. Hussain, and Y. L. Chen, Discovery of a three-dimensional topological Dirac semimetal, Na$_3$Bi, Science **343**, 864 (2014).